

Supersymmetry dynamics on Rydberg atom arrays

Shuo Liu,^{1,*} Zhengzhi Wu,^{1,2,*} Shi-Xin Zhang,^{3,†} and Hong Yao^{1,‡}

¹*Institute for Advanced Study, Tsinghua University, Beijing 100084, China*

²*Rudolf Peierls Centre for Theoretical Physics, Parks Road, Oxford, OX1 3PU, UK*

³*Institute of Physics, Chinese Academy of Sciences, Beijing 100190, China*

(Dated: July 9, 2025)

Spacetime supersymmetry (SUSY) that interchanges fermions and bosons is of great theoretical importance but has not yet been revealed experimentally in particle physics. It has also been desired to explore quantum-mechanical SUSY in microscopic lattice models. Inspired by the recent experiments of Floquet engineering of Rydberg atom arrays, we propose to simulate quantum mechanical supersymmetric model and realize quantum mechanical SUSY in Floquet Rydberg atom arrays. Moreover, we utilize the supercharge dynamics to demonstrate the SUSY property of the model under investigation: the expectation value of supercharge freezes under time evolution for supersymmetric lattice models in contrast to the trivial oscillation for generic nonsupersymmetric lattice models. The proposal is validated on direct simulation of Rydberg atom arrays' dynamics and ready for experiments. This work sheds light on the future experimental exploration of SUSY with the help of Rydberg atom arrays.

Introduction.— The concept of spacetime supersymmetry (SUSY) [1, 2], which postulates a symmetry interchanging fermions and bosons, offers a compelling way to address various fundamental and long-standing problems, including the hierarchy problem in particle physics [3] and cosmological constant problem [4]. However, despite extensive research efforts, there has been no conclusive experimental evidence to date for SUSY and its spontaneous breaking within the realm of particle physics.

On a different front, it is well known that spacetime SUSY might emerge at low energies in many-body systems at criticality. For instance, the spacetime SUSY could emerge at 1+1 dimensional tricritical Ising transition [5, 6]. Emergent SUSY at quantum criticality and the associated microscopic models have been extensively investigated [7–28]. Even so, the experimental confirmation of the emergent spacetime SUSY remains elusive. On one hand, investigating the ground state properties presents a significant challenge for existing experimental platforms, particularly when attempting to achieve emergent SUSY at a multicritical point, which requires fine-tuning of more than one parameter and adiabatic annealing. On the other hand, to accurately characterize SUSY, it is essential to employ unconventional measurement methods [29–32] capable of detecting the non-local string operators that are intrinsic to fermionic modes.

Apart from lattice models with emergent spacetime SUSY, lattice models with explicit quantum-mechanical SUSY can be constructed [33–44]. One well-known family of supersymmetric lattice models is the M_k model [34] which describes 1D fermion chain under the constraint that at most k consecutive sites may be occupied and thus restricting the hopping. Explicit quantum-mechanical SUSY of a lattice model can induce a non-trivial energy spectrum – all its eigenstates form either singlet or doublet representation of the SUSY algebra. The singlet corresponds to the supersymmetric ground

state with eigenenergy $E = 0$, while each doublet includes two eigenstates with the same eigenenergy $E > 0$. The fermion numbers of two eigenstates in each doublet differ by 1 and thus these two eigenstates correspond to fermionic and bosonic modes, respectively. Consequently, the supersymmetric lattice model also exhibits unique dynamical features which could be more experimental accessible than the ground state properties in a variety of quantum simulator platforms.

Rydberg atom arrays serve as a powerful and flexible platform for processing quantum information [45–52], exploring exotic phases of matter and simulating novel quantum dynamics [53–63]. Recently, a Floquet engineering scheme of blockade-consistent spin-exchange interactions in periodically driven Rydberg atom arrays has been proposed [64], naturally resembling the constraint in supersymmetric M_k models [34] and indicating the potential of utilizing Rydberg atom arrays to construct non-trivial interactions in quantum many-body systems. With the Floquet engineering toolbox on Rydberg atom arrays, it is important and urgent to explore the new possibility of experimentally demonstrating SUSY.

In this Letter, we find that quantum-mechanical SUSY can be realized in Floquet Rydberg atom arrays by tuning pulse parameters, inspired by the recent Floquet engineering of Rydberg atom arrays [64]. We further propose to experimentally investigate the supersymmetry dynamics under the Floquet engineering [64–80]. Specifically, we demonstrate that the effective Floquet Hamiltonian of the Rydberg atom array can be tuned to the supersymmetric M_1 model [33] on an open-boundary chain, which is the simplest one in the family of supersymmetric M_k models. Moreover, we propose to characterize the SUSY dynamics by the evolution of the supercharge which has friendly experimental requirements in terms of state preparation and measurements. The supersymmetric Hamiltonian with the frozen supercharge

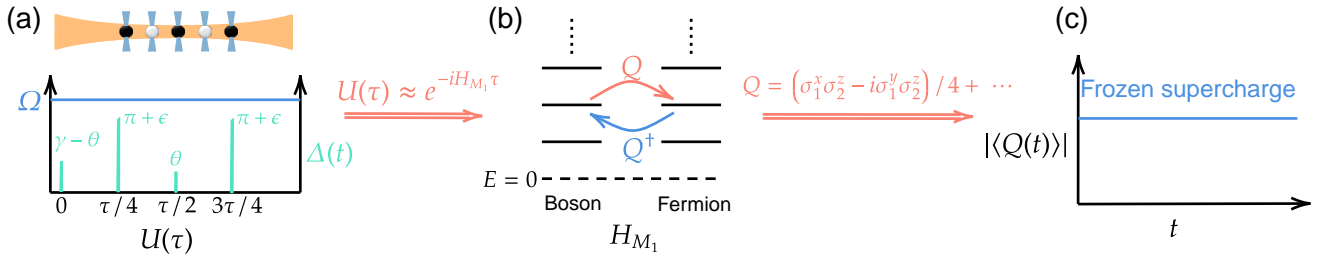


FIG. 1. Simulating supersymmetry dynamics on Rydberg atom arrays. (a) Upper panel: Rydberg atom arrays within optical tweezers. The degree of freedom at each site comprises the atomic ground state ($|g\rangle$, black solid circle) and the Rydberg state (highly excited state $|r\rangle$, white solid circle). Lower panel: the time evolution within one period τ and the unitary evolution operator over one period is given by $U(\tau)$ (see Eq. (9)). Firstly, we utilize the PXP model as an approximate description of Rydberg atoms and the static Hamiltonian is $H_{\text{PXP}}^{\text{bc}} = \sigma_1^x P_2^r + \sum_{i=2}^{L-1} P_{i-1}^r \sigma_i^x P_{i+1}^r + P_L^r \sigma_L^x$ whose strength is denoted as Rabi frequency Ω (blue line). The four green peaks represent the global detunings at times $0, \tau/4, \tau/2, 3\tau/4$, respectively. The strength of the global detuning, i.e., the height of the peak, is parameterized by γ, θ, ϵ and tunable. (b) Secondly, by employing suitable Floquet engineering as discussed in the main text, we achieve a Floquet effective Hamiltonian that mirrors the supersymmetric M_1 model. It is a supersymmetric lattice model and the eigenstates with $E > 0$ naturally form doublets, giving two degenerate states with different fermion parity. (c) Lastly, we employ the expectation value of the supercharge operator to investigate the supersymmetry dynamics. Notably, the dynamics of the supercharge operator is a constant under the quench of a supersymmetric Hamiltonian.

dynamics can be distinguished from other nonsupersymmetric Hamiltonians where the supercharge dynamics is nonconserved. We have also numerically demonstrated the non-trivial supersymmetry dynamics using both effective Hamiltonian and the original Rydberg atom array dynamics and analyzed the effects of nonsupersymmetric perturbations. The main results are summarized in Fig. 1. Besides supercharge dynamics, this scheme can be directly applied to investigate the dynamics of the supersymmetric lattice model characterized by other observables. This provides a pathway to explore other intriguing dynamics related to SUSY such as the weak ergodicity breaking from supersymmetry [81].

The M_1 model and supersymmetry dynamics.—We consider the one-dimensional M_1 model [33], which is one of the most famous $\mathcal{N} = 2$ supersymmetric lattice model, with the following Hamiltonian

$$H_{M_1} = \{Q, Q^\dagger\}. \quad (1)$$

$Q = \sum_i Q_i$ is the nilpotent supercharge satisfying $Q^2 = 0$, where $Q_i = (-1)^i P_{i-1} c_i^\dagger P_{i+1}$ with c_i^\dagger and $P_i \equiv 1 - c_i^\dagger c_i$ being the fermion creation operator and projection operator to vacuum state at site i . Obviously, $[Q, H_{M_1}] = [Q^\dagger, H_{M_1}] = 0$; namely the lattice Hamiltonian in Eq. (1) explicitly processes the supersymmetry. Moreover, based on the construction of Hamiltonian, the eigenvalues are non-negative and thus an eigenstate $|G\rangle$ with $E = 0$ must be a ground state, which is dubbed as supersymmetric ground state satisfying $Q|G\rangle = Q^\dagger|G\rangle = 0$. Other eigenstates with $E > 0$ form doublet representations. Each doublet includes two eigenstates: $|s\rangle$ and $Q|s\rangle$, satisfying $Q^\dagger|s\rangle = 0$ and $Q(Q|s\rangle) = 0$. Moreover, $Q|s\rangle$ is the superpartner of $|s\rangle$ sharing the same eigenenergy yet exhibiting a distinct fermion parity as supercharge operator

Q effectively adds a fermion into the system. Consequently, two eigenstates in each doublet can be regarded as the fermionic and bosonic modes, respectively, which is a hallmark of quantum-mechanical SUSY. The number of supersymmetric ground states depends on the choice of system size and boundary conditions (see Ref. [34] for detailed discussion). In the following, we focus on the case with system size $L = 3l + 1$ and open boundary conditions (OBC). There is no supersymmetric ground state, nevertheless, all the eigenstates can still be decomposed into doublets under SUSY.

Owing to the presence of explicit quantum-mechanical SUSY in the M_1 model, we aim to extract nontrivial features unique to SUSY from quantum dynamics. The experimental demonstration of SUSY dynamics will provide a practical and meaningful task for current quantum devices to achieve an advantage beyond the reach of the classical simulation. For instance, the quench dynamics for a generic Hamiltonian vary significantly depending on initial states while the dynamics starting from a certain initial state are the same as those starting from its superpartner guaranteed by the supersymmetry [82]. Therefore, the observation of identical quantum dynamics from two initial states serves as compelling evidence for the existence of SUSY. However, akin to the unrealized experimental exploration of spacetime SUSY in low energy, simulating SUSY dynamics poses a significant challenge due to the difficulty in preparing the superpartner of a generic state and thus the experimental investigations are severely limited (see Supplemental Materials (SM) for more details [83]).

To address this limitation, we propose to directly investigate the dynamics of the expectation value of super-

charge operator Q

$$\langle Q(t) \rangle = \langle \psi(0) | e^{iHt} Q e^{-iHt} | \psi(0) \rangle, \quad (2)$$

to reveal the supersymmetry, where $|\psi(0)\rangle$ is an arbitrary initial state and H is a generic Hamiltonian. When H is supersymmetric, for instance $H = H_{M_1}$ and $[Q, H] = 0$, the supercharge dynamics freeze,

$$\langle Q(t) \rangle = \langle \psi(0) | Q | \psi(0) \rangle = \langle Q(0) \rangle = c, \quad (3)$$

where c is an initial-state dependent (complex) constant. In contrast, $\langle Q(t) \rangle$ will be nonconserved for a generic Hamiltonian that does not respect SUSY. Consequently, the frozen supercharge dynamics serve as a decisive signal for the presence of SUSY, and no high-precision initial state preparation is required. More importantly, as detailed below, both the analog simulation of the M_1 model and the estimation of the expectation value of the supercharge operator can be easily realized on Rydberg atom arrays.

In the following, we shall focus on the M_1 model with OBC denoted as $H_{M_1}^{\text{obc}}$. With the help of the Jordan-Wigner transformation and particle-hole transformation, the M_1 model in the spin-1/2 basis can be rewritten as

$$\begin{aligned} H_{M_1}^{\text{obc}} = & \frac{1}{4} H_{\text{ZIZ}}^{\text{obc}} - H_{\text{PXP}}^{\text{obc}} - N \\ & + \frac{1}{2} (n_1^r - n_2^r - n_{L-1}^r + n_L^r), \end{aligned} \quad (4)$$

where $H_{\text{ZIZ}}^{\text{obc}}$ is the next-nearest-neighbor ZZ interaction $H_{\text{ZIZ}}^{\text{obc}} = \sum_{j=2}^{L-1} \sigma_j^z \sigma_{j+1}^z$, $H_{\text{PXP}}^{\text{obc}}$ is the blockaded nearest-neighbor spin-exchange interaction $H_{\text{PXP}}^{\text{obc}} = \frac{1}{2} (\sigma_1^x \sigma_2^x + \sigma_1^y \sigma_2^y) P_3^r + \frac{1}{2} \sum_{j=2}^{L-2} P_{j-1}^r (\sigma_j^x \sigma_{j+1}^x + \sigma_j^y \sigma_{j+1}^y) P_{j+2}^r + \frac{1}{2} P_{L-2}^r (\sigma_{L-1}^x \sigma_L^x + \sigma_{L-1}^y \sigma_L^y)$, and N is the number operator $N = \sum_{j=1}^L n_j^r$ with $P_i^r = \frac{\mathbb{I} + \sigma_i^z}{2}$ and $n_i^r = \frac{\mathbb{I} - \sigma_i^z}{2}$. Here $\sigma_i^{(x,y,z)}$ are Pauli matrix on site i . As shown below, the local spin-1/2 Hilbert space can be formed by the Rydberg atom's analog basis $|g\rangle$ and $|r\rangle$, representing ground and Rydberg states, respectively. $P_i^r = |g\rangle\langle g|_i$ is the projection operator to the ground state $|g\rangle$ on site i while $n_i^r = |r\rangle\langle r|_i$ projects to the Rydberg state. Moreover, the supercharge operator Q corresponds to a summation of Pauli string operators: $Q = \frac{\sigma_1^-}{2} \frac{\mathbb{I} + \sigma_2^z}{2} + \sum_{i=2}^{L-1} \frac{\mathbb{I} + \sigma_{i-1}^z}{2} \left(\frac{\sigma_i^-}{2} \prod_{j=1}^{i-1} (-\sigma_j^z) \right) \frac{\mathbb{I} + \sigma_{i+1}^z}{2} + \frac{\mathbb{I} + \sigma_{L-1}^z}{2} \left(\frac{\sigma_L^-}{2} \prod_{j=1}^{L-1} (-\sigma_j^z) \right)$. See SM for more details [83].

Experimental implementation.—Recently, Floquet engineering of blockaded spin-exchange interaction in periodically driven Rydberg chains has been proposed and utilized for the exploration of gapless Luttinger liquid phase [64]. Inspired by this construction, we harness the potential of Floquet engineering and propose to experimentally simulate the supercharge dynamics of the supersymmetric M_1 model on Rydberg atom arrays.

For simplicity, we consider the following driven PXP model with OBC

$$H^{\text{obc}}(t) = \frac{\Omega}{2} H_{\text{PXP}}^{\text{obc}} - \Delta_0(t) N - \tilde{\Delta}(t) N, \quad (5)$$

where

$$H_{\text{PXP}}^{\text{obc}} = \sigma_1^x P_2^r + \sum_{i=2}^{L-1} P_{i-1}^r \sigma_i^x P_{i+1}^r + P_{L-1}^r \sigma_L^x, \quad (6)$$

is the pure PXP Hamiltonian, which describes the blockade mechanism in a chain of Rydberg atoms and the effect of sandwiching the Pauli X operators on each site between projectors is that the state of an atom can flip between the ground state and Rydberg state only if both adjacent atoms are in the ground states. Here, $\Delta_0(t)$ and $\tilde{\Delta}(t)$ are the time-dependent global detunings given by

$$\Delta_0(t) = \pi \sum_n \delta(t - \frac{\tau}{4} - n \frac{\tau}{2}), \quad (7)$$

$$\begin{aligned} \tilde{\Delta}(t) = & (\gamma - \theta) \sum_n \delta(t - n\tau) + \theta \sum_n \delta(t - \frac{\tau}{2} - n\tau) \\ & + \epsilon \sum_n \delta(t - \frac{\tau}{4} - n\tau) + \epsilon \sum_n \delta(t - \frac{3\tau}{4} - n\tau), \end{aligned} \quad (8)$$

with τ being the Floquet period and γ, θ, ϵ being the controllable strengths of global detuning perturbations. The corresponding time evolution unitary for one period is

$$\begin{aligned} U(\tau) = & \mathcal{T} e^{-i \int_0^\tau dt H^{\text{obc}}(t)} \\ = & U_{\text{PXP}} V_N(\epsilon + \pi) U_{\text{PXP}} V_N(\theta) \\ & U_{\text{PXP}} V_N(\epsilon + \pi) U_{\text{PXP}} V_N(\gamma - \theta), \end{aligned} \quad (9)$$

where

$$U_{\text{PXP}} = e^{-i \frac{\tau}{4} \frac{\Omega}{2} H_{\text{PXP}}^{\text{obc}}}, \quad V_N(\beta) = e^{i \beta N}. \quad (10)$$

It can be shown that Floquet unitary $U_F \equiv U(\tau)$ can be approximately described by a time-independent effective Floquet Hamiltonian H_F , i.e.,

$$U_F \approx e^{-i H_F \tau}, \quad (11)$$

and thus the stroboscopic dynamics ($t = n\tau, n \in \mathbb{N}$) corresponds to the time evolution under H_F : $U(n\tau) = (U_F)^n \approx e^{-i H_F n\tau}$. With small detuning perturbations $(\epsilon, \gamma, \theta)$, one can obtain the effective Floquet Hamiltonian H_F through a Floquet-Magnus expansion [84, 85]: $H_F = H_F^{(0)} + H_F^{(1)} + \mathcal{O}(\epsilon^3)$.

When $\frac{\Omega\tau}{4} \ll 1$,

$$H_F^{(0)} = \frac{h}{4} H_{\text{ZIZ}}^{\text{obc}} - h H_{\text{PXP}}^{\text{obc}} - J N, \quad (12)$$

$$+ \frac{h}{2} (n_1^r - n_2^r - n_{N-1}^r + n_N^r)$$

$$H_F^{(1)} = g H_{\text{PXP}}^{\text{obc}}, \quad (13)$$

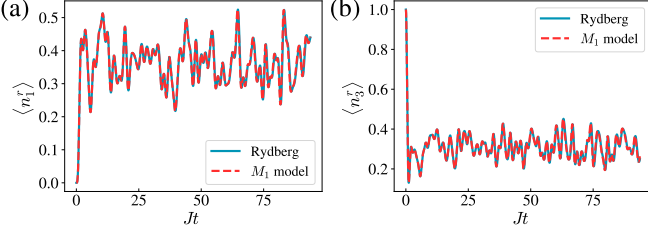


FIG. 2. The dynamics of Rydberg state density on site 1 (a) and site 3 (b), respectively. Here, we set $L = 13$, $\tau = 0.001$, $\frac{\Omega\tau}{4} = 0.025$, $\epsilon = -0.1$. The numerical results evolved by the M_1 model (red) agree well with those evolved by the Floquet unitary U_F (blue).

where

$$J = \frac{\gamma + 2\epsilon}{\tau} - \frac{3\epsilon\Omega^2\tau}{32}, \quad (14)$$

$$h = -\frac{\epsilon\Omega^2\tau}{32}, \quad (15)$$

$$g = -\frac{\epsilon(\epsilon + \theta)\Omega}{8}. \quad (16)$$

See the SM [83] for more details and Ref. [64] for the derivation with periodic boundary conditions. Furthermore, when $\epsilon/\Omega\tau \ll 1$, the contribution of the $H_F^{(1)}$ becomes negligible. In this case, it is permissible to set θ to zero, thereby considering only the three global detuning perturbations that occur over each period. More importantly, when $\gamma = \epsilon(\frac{\Omega^2\tau^2}{16} - 2)$, i.e. $J = h$, we have

$$H_F \approx H_F^{(0)} = \frac{J}{4}H_{\text{ZIZ}}^{\text{obc}} - JH_{\text{PXP}}^{\text{obc}} - JN \quad (17)$$

$$+ \frac{J}{2}(n_1^r - n_2^r - n_{N-1}^r + n_N^r),$$

and thus the zeroth-order H_F is exactly the same as the Hamiltonian of the supersymmetric M_1 model as shown in Eq. (4) up to an unimportant overall factor J . Therefore, the driven PXP model under Floquet engineering with suitable parameters can describe the quantum dynamics of the supersymmetric M_1 model. We note that the first-order correction term $H_F^{(1)}$ does not preserve the quantum-mechanical SUSY property. However, it is possible to tune $\theta = -\epsilon$ to eliminate the H_{PXP} term, thereby ensuring that the effective Floquet Hamiltonian retains SUSY up to this order. In the following, we set $\gamma = \epsilon(\frac{\Omega^2\tau^2}{16} - 2)$ and $\theta = -\epsilon$ unless other specified.

To validate the correspondence between the stroboscopic dynamics of the driven PXP model under Floquet engineering (Eq. (9)) and the supersymmetric M_1 model, we use the python package `TensorCircuit` [86] to perform numerical simulations. We calculate the density dynamics of Rydberg states on different sites. The system size

is chosen as $L = 3l + 1$ and the initial state is chosen as

$$|K_1\rangle = \left(\prod_{j=1}^l \sigma_{3j}^x \right) |g\rangle^{\otimes L}. \quad (18)$$

As illustrated in Fig. 2, the Rydberg state density dynamics evolved by Floquet unitary U_F coincide with those evolved by the M_1 model. In addition, we have also calculated the dynamics of the correlation function and tested other initial states (see more numerical results in the SM [83]). The results also agree well with those of the M_1 model. Therefore, the effective Floquet Hamiltonian is a good approximation of the M_1 model. We note that the accumulated approximation errors will induce the deviation at late times.

Supercharge dynamics.—Having demonstrated the effectiveness of simulating the real-time evolution of M_1 model by the driven PXP model tuned to the SUSY point, we then investigate the supersymmetry dynamics characterized by the expectation value of supercharge $\langle Q(t) \rangle$.

We note that the initial state should be easily prepared on Rydberg atom arrays, yielding a superposition of eigenstates mixing different fermion-parity sectors to ensure a non-zero $\langle Q(t) \rangle$. To prepare the initial state, we first let the state $|K_1\rangle$ (see Eq. (18), or any other easily prepared state) evolve with pure PXP Hamiltonian $H_{\text{PXP}}^{\text{obc}}$ breaking the parity symmetry to time t^* . We choose

$$|\psi(0)\rangle = e^{-iH_{\text{PXP}}^{\text{obc}}t^*} |K_1\rangle \quad (19)$$

as the initial state for the supersymmetry dynamics and turn on the Floquet engineering at t^* . Then $|\psi(0)\rangle$ is evolved by the Floquet unitary U_F and thus $|\psi(n\tau)\rangle = (U_F)^n |\psi(0)\rangle$.

As illustrated in Eq. (17), the effective Floquet Hamiltonian H_F is supersymmetric when $\theta = -\epsilon$ and $\gamma = \epsilon(\frac{\Omega^2\tau^2}{16} - 2)$. Here, we set $\theta = -(1 + \delta)\epsilon$ and use δ to describe the deviation away from the supersymmetric point. The numerical results of supercharge dynamics with different initial states are shown in Fig. 3. When $\delta = 0$, the effective Floquet Hamiltonian is the same as the M_1 Hamiltonian and the expectation value of the supercharge remains unchanged. In contrast, when $\delta > 0$, the effective Floquet Hamiltonian is not supersymmetric anymore and then there exist decays and oscillations in supercharge dynamics.

Furthermore, to experimentally demonstrate the supersymmetry dynamics of the M_1 model, two issues must be addressed. Firstly, in the experiment, the Rydberg atoms actually interact via van der Waals interaction with blockade radius R_b and the global detuning pulses have finite widths. Previous work [64] has validated the good agreement between the results of the driven PXP model and the model of driven Rydberg atom arrays with long-range interactions. Therefore, we believe that the

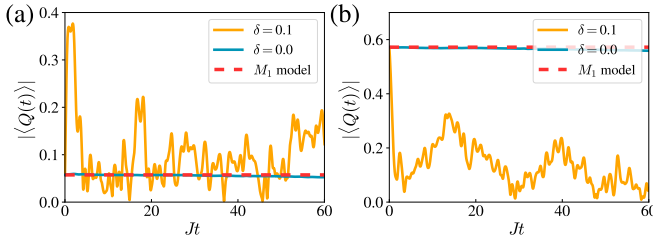


FIG. 3. Supercharge dynamics with (a) $t^* = 5$ and (b) $t^* = 10$. Here, we set $L = 13$, $\tau = 0.001$, $\frac{\Omega\tau}{4} = 0.025$, $\epsilon = -0.1$, and $\theta = -(1 + \delta)\epsilon$. When $\delta = 0.0$ the expectation value of supercharge is a constant and is the same as that under the quench of supersymmetric M_1 model, indicating the effective Floquet Hamiltonian feature a quantum-mechanical SUSY. However, when $\delta > 0$ the supercharge dynamics exhibit oscillation, i.e., the effective Floquet Hamiltonian is non-supersymmetric. We note that the accumulated Floquet engineering approximation errors induce the deviation at late times even for $\delta = 0$.

corresponding effective Floquet Hamiltonian in the real experiment platform can still act as a good approximation of the supersymmetric M_1 model. Secondly, the measurement of supercharge should be friendly for the Rydberg atom arrays. Via the quantum analog-to-digital converter [47, 87], one can transform from the analog basis to the digital basis where the measurement of any Pauli string is easy via proper single qubit rotations and computational basis measurements.

Discussion and outlook.— In conclusion, we have revealed that the supersymmetric M_1 model can be realized on Rydberg atom arrays via Floquet engineering by choosing appropriate parameters. We further proposed to uncover the supersymmetry dynamics via the supercharge expectation value and have demonstrated the frozen supercharge dynamics for supersymmetric Hamiltonian. This scheme is suitable for experimental demonstration on current Rydberg atom arrays.

It would be intriguing to explore the Floquet engineering scheme to achieve M_1 model with higher precision. Besides the supersymmetry dynamics of the one-dimensional M_1 model, it is worth further investigating the quantum simulation in higher dimensions or for other supersymmetric lattice models. More importantly, the current Floquet engineering scheme uses only global detunings. It is essential to extend Floquet engineering to the case with site-dependent detuning fields [88], which is helpful for constructing other nontrivial interactions. Furthermore, due to the flexibility of the Floquet engineering, it is promising to prepare the ground state of the supersymmetric M_1 model via adiabatic evolution, and thus experimentally identify the spacetime SUSY in low energy regime of the M_1 model and other related models [89], which shall provide significant light into the understanding of spacetime SUSY and its breaking.

Acknowledgements.— We acknowledge Cheng Chen,

Shao-Kai Jian, Zi-Xiang Li, and Shuai Yin, and especially Paul Fendley for helpful discussions. This work was supported in part by NSFC under Grants No. 12347107 and No.12334003 (S.L. and H.Y.), by MOSTC under Grant No.2021YFA1400100 (H.Y.), and by the Xplorer Prize through the New Cornerstone Science Foundation (H.Y.). S.-X.Z. acknowledges the support from Innovation Program for Quantum Science and Technology (2024ZD0301700) and the start-up grant at IOP-CAS. Z.W. acknowledges the support in part from Shuimu fellowships at Tsinghua University and the EPSRC under grant EP/X030881/1.

* These two authors contributed equally to this work.

† shixinzhang@iphy.ac.cn

‡ yaohong@tsinghua.edu.cn

- [1] J.-L. Gervais and B. Sakita, Field theory interpretation of supergauges in dual models, *Nuclear Physics B* **34**, 632 (1971).
- [2] J. Wess and B. Zumino, Supergauge transformations in four dimensions, *Nuclear Physics B* **70**, 39 (1974).
- [3] S. Dimopoulos and H. Georgi, Softly broken supersymmetry and $su(5)$, *Nuclear Physics B* **193**, 150 (1981).
- [4] E. Cremmer, S. Ferrara, C. Kounnas, and D. Nanopoulos, Naturally vanishing cosmological constant in $n=1$ supergravity, *Physics Letters B* **133**, 61 (1983).
- [5] D. Friedan, Z. Qiu, and S. Shenker, Superconformal invariance in two dimensions and the tricritical ising model, *Physics Letters B* **151**, 37 (1985).
- [6] A. B. Zamolodchikov, Conformal Symmetry and Multicritical Points in Two-Dimensional Quantum Field Theory. (In Russian), *Sov. J. Nucl. Phys.* **44**, 529 (1986).
- [7] D. Friedan, Z. Qiu, and S. Shenker, Conformal invariance, unitarity, and critical exponents in two dimensions, *Phys. Rev. Lett.* **52**, 1575 (1984).
- [8] L. Balents, M. P. A. Fisher, and C. Nayak, Nodal liquid theory of the pseudo-gap phase of high- t_c superconductors, *International Journal of Modern Physics B* **12**, 1033 (1998).
- [9] S.-S. Lee, Emergence of supersymmetry at a critical point of a lattice model, *Phys. Rev. B* **76**, 075103 (2007).
- [10] Y. Yu and K. Yang, Supersymmetry and the goldstino-like mode in bose-fermi mixtures, *Phys. Rev. Lett.* **100**, 090404 (2008).
- [11] I. F. Herbut, V. Jurić, and O. Vafek, Relativistic mott criticality in graphene, *Phys. Rev. B* **80**, 075432 (2009).
- [12] Y. Yu and K. Yang, Simulating the wess-zumino supersymmetry model in optical lattices, *Phys. Rev. Lett.* **105**, 150605 (2010).
- [13] M. Z. Hasan and C. L. Kane, Colloquium: Topological insulators, *Rev. Mod. Phys.* **82**, 3045 (2010).
- [14] X.-L. Qi and S.-C. Zhang, Topological insulators and superconductors, *Rev. Mod. Phys.* **83**, 1057 (2011).
- [15] B. Bauer, L. Huijse, E. Berg, M. Troyer, and K. Schoutens, Supersymmetric multicritical point in a model of lattice fermions, *Phys. Rev. B* **87**, 165145 (2013).
- [16] B. Roy, V. Jurić, and I. F. Herbut, Quantum superconducting criticality in graphene and topological insulators,

- Phys. Rev. B* **87**, 041401 (2013).
- [17] T. Grover, D. N. Sheng, and A. Vishwanath, Emergent space-time supersymmetry at the boundary of a topological phase, *Science* **344**, 280 (2014).
- [18] P. Ponte and S.-S. Lee, Emergence of supersymmetry on the surface of three-dimensional topological insulators, *New Journal of Physics* **16**, 013044 (2014).
- [19] L. Huijse, B. Bauer, and E. Berg, Emergent supersymmetry at the ising-berezinskii-kosterlitz-thouless multicritical point, *Phys. Rev. Lett.* **114**, 090404 (2015).
- [20] S.-K. Jian, Y.-F. Jiang, and H. Yao, Emergent space-time supersymmetry in 3d weyl semimetals and 2d dirac semimetals, *Phys. Rev. Lett.* **114**, 237001 (2015).
- [21] A. Rahmani, X. Zhu, M. Franz, and I. Affleck, Emergent supersymmetry from strongly interacting majorana zero modes, *Phys. Rev. Lett.* **115**, 166401 (2015).
- [22] T. H. Hsieh, G. B. Halász, and T. Grover, All majorana models with translation symmetry are supersymmetric, *Phys. Rev. Lett.* **117**, 166802 (2016).
- [23] S.-K. Jian, C.-H. Lin, J. Maciejko, and H. Yao, Emergence of supersymmetric quantum electrodynamics, *Phys. Rev. Lett.* **118**, 166802 (2017).
- [24] Z.-X. Li, Y.-F. Jiang, and H. Yao, Edge quantum criticality and emergent supersymmetry in topological phases, *Phys. Rev. Lett.* **119**, 107202 (2017).
- [25] Z.-X. Li, A. Vaezi, C. B. Mendl, and H. Yao, Numerical observation of emergent spacetime supersymmetry at quantum criticality, *Science Advances* **4**, eaau1463 (2018).
- [26] E. O'Brien and P. Fendley, Lattice supersymmetry and order-disorder coexistence in the tricritical ising model, *Phys. Rev. Lett.* **120**, 206403 (2018).
- [27] K. K. W. Ma, R. Wang, and K. Yang, Realization of supersymmetry and its spontaneous breaking in quantum hall edges, *Phys. Rev. Lett.* **126**, 206801 (2021).
- [28] C. Li, S. Liu, H. Wang, W. Zhang, Z.-X. Li, H. Zhai, and Y. Gu, Uncovering emergent spacetime supersymmetry with rydberg atom arrays, *Phys. Rev. Lett.* **133**, 223401 (2024).
- [29] M. Endres, M. Cheneau, T. Fukuhara, C. Weitenberg, P. Schauß, C. Gross, L. Mazza, M. C. Bañuls, L. Pollet, I. Bloch, and S. Kuhr, Observation of correlated particle-hole pairs and string order in low-dimensional mott insulators, *Science* **334**, 200 (2011).
- [30] T. A. Hilker, G. Salomon, F. Grusdt, A. Omran, M. Boll, E. Demler, I. Bloch, and C. Gross, Revealing hidden antiferromagnetic correlations in doped hubbard chains via string correlators, *Science* **357**, 484 (2017).
- [31] C. S. Chiu, G. Ji, A. Bohrdt, M. Xu, M. Knap, E. Demler, F. Grusdt, M. Greiner, and D. Greif, String patterns in the doped hubbard model, *Science* **365**, 251 (2019).
- [32] S. de Léseleuc, V. Lienhard, P. Scholl, D. Barredo, S. Weber, N. Lang, H. P. Büchler, T. Lahaye, and A. Browaeys, Observation of a symmetry-protected topological phase of interacting bosons with rydberg atoms, *Science* **365**, 775 (2019).
- [33] P. Fendley, K. Schoutens, and J. de Boer, Lattice models with $\mathcal{N} = 2$ supersymmetry, *Phys. Rev. Lett.* **90**, 120402 (2003).
- [34] P. Fendley, B. Nienhuis, and K. Schoutens, Lattice fermion models with supersymmetry, *Journal of Physics A: Mathematical and General* **36**, 12399 (2003).
- [35] X. Yang and P. Fendley, Non-local spacetime supersymmetry on the lattice, *Journal of Physics A: Mathematical and General* **37**, 8937 (2004).
- [36] P. Fendley and K. Schoutens, Exact results for strongly correlated fermions in 2 + 1 dimensions, *Phys. Rev. Lett.* **95**, 046403 (2005).
- [37] L. Huijse, J. Halverson, P. Fendley, and K. Schoutens, Charge frustration and quantum criticality for strongly correlated fermions, *Phys. Rev. Lett.* **101**, 146406 (2008).
- [38] L. Huijse, N. Moran, J. Vala, and K. Schoutens, Exact ground states of a staggered supersymmetric model for lattice fermions, *Phys. Rev. B* **84**, 115124 (2011).
- [39] L. Huijse, D. Mehta, N. Moran, K. Schoutens, and J. Vala, Supersymmetric lattice fermions on the triangular lattice: superfrustration and criticality, *New Journal of Physics* **14**, 073002 (2012).
- [40] C. Li, E. Lantagne-Hurtubise, and M. Franz, Supersymmetry in an interacting majorana model on the kagome lattice, *Phys. Rev. B* **100**, 195146 (2019).
- [41] A. Prakash and J. Wang, Boundary supersymmetry of (1 + 1)D fermionic symmetry-protected topological phases, *Phys. Rev. Lett.* **126**, 236802 (2021).
- [42] A. Prakash and J. Wang, Unwinding fermionic symmetry-protected topological phases: Supersymmetry extension, *Phys. Rev. B* **103**, 085130 (2021).
- [43] M.-L. Cai, Y.-K. Wu, Q.-X. Mei, W.-D. Zhao, Y. Jiang, L. Yao, L. He, Z.-C. Zhou, and L.-M. Duan, Observation of supersymmetry and its spontaneous breaking in a trapped ion quantum simulator, *Nature Communications* **13**, 3412 (2022).
- [44] P. H. Wilhelm, Y. H. Kwan, A. M. Läuchli, and S. A. Parameswaran, Supersymmetry on the honeycomb lattice: Resonating charge stripes, superfrustration, and domain walls, *Phys. Rev. B* **110**, 165124 (2024).
- [45] M. Saffman, T. G. Walker, and K. Mølmer, Quantum information with rydberg atoms, *Rev. Mod. Phys.* **82**, 2313 (2010).
- [46] M. Morgado and S. Whitlock, Quantum simulation and computing with Rydberg-interacting qubits, *AVS Quantum Science* **3**, 023501 (2021).
- [47] D. Bluvstein, H. Levine, G. Semeghini, T. T. Wang, S. Ebadi, M. Kalinowski, A. Keesling, N. Maskara, H. Pichler, M. Greiner, V. Vuletić, and M. D. Lukin, A quantum processor based on coherent transport of entangled atom arrays, *Nature* **604**, 451 (2022).
- [48] S. Ma, G. Liu, P. Peng, B. Zhang, S. Jandura, J. Claes, A. P. Burgers, G. Pupillo, S. Puri, and J. D. Thompson, High-fidelity gates and mid-circuit erasure conversion in an atomic qubit, *Nature* **622**, 279 (2023).
- [49] P. Scholl, A. L. Shaw, R. B.-S. Tsai, R. Finkelstein, J. Choi, and M. Endres, Erasure conversion in a high-fidelity Rydberg quantum simulator, *Nature* **622**, 273 (2023).
- [50] K. Singh, C. E. Bradley, S. Anand, V. Ramesh, R. White, and H. Bernien, Mid-circuit correction of correlated phase errors using an array of spectator qubits, *Science* **380**, 1265 (2023).
- [51] D. Bluvstein, S. J. Evered, A. A. Geim, S. H. Li, H. Zhou, T. Manovitz, S. Ebadi, M. Cain, M. Kalinowski, D. Hangleiter, J. P. Bonilla Ataides, N. Maskara, I. Cong, X. Gao, P. Sales Rodriguez, T. Karolyshyn, G. Semeghini, M. J. Gullans, M. Greiner, V. Vuletić, and M. D. Lukin, Logical quantum processor based on reconfigurable atom arrays, *Nature* **626**, 58 (2024).
- [52] Q. Xu, J. P. Bonilla Ataides, C. A. Pattison, N. Raveendran, D. Bluvstein, J. Wurtz, B. Vasić, M. D. Lukin,

- L. Jiang, and H. Zhou, Constant-overhead fault-tolerant quantum computation with reconfigurable atom arrays, *Nature Physics* **20**, 1084 (2024).
- [53] H. Bernien, S. Schwartz, A. Keesling, H. Levine, A. Omran, H. Pichler, S. Choi, A. S. Zibrov, M. Endres, M. Greiner, V. Vuletić, and M. D. Lukin, Probing many-body dynamics on a 51-atom quantum simulator, *Nature* **551**, 579 (2017).
- [54] A. Browaeys and T. Lahaye, Many-body physics with individually controlled Rydberg atoms, *Nature Physics* **16**, 132 (2020).
- [55] S. Ebadi, T. T. Wang, H. Levine, A. Keesling, G. Semeghini, A. Omran, D. Bluvstein, R. Samajdar, H. Pichler, W. W. Ho, S. Choi, S. Sachdev, M. Greiner, V. Vuletić, and M. D. Lukin, Quantum phases of matter on a 256-atom programmable quantum simulator, *Nature* **595**, 227 (2021).
- [56] P. Scholl, M. Schuler, H. J. Williams, A. A. Eberharter, D. Barredo, K.-N. Schymik, V. Lienhard, L.-P. Henry, T. C. Lang, T. Lahaye, A. M. Läuchli, and A. Browaeys, Quantum simulation of 2D antiferromagnets with hundreds of Rydberg atoms, *Nature* **595**, 233 (2021).
- [57] X. Wu, X. Liang, Y. Tian, F. Yang, C. Chen, Y.-C. Liu, M. K. Tey, and L. You, A concise review of rydberg atom based quantum computation and quantum simulation*, *Chinese Physics B* **30**, 020305 (2021).
- [58] D. Bluvstein, A. Omran, H. Levine, A. Keesling, G. Semeghini, S. Ebadi, T. T. Wang, A. A. Michailidis, N. Maskara, W. W. Ho, S. Choi, M. Serbyn, M. Greiner, V. Vuletić, and M. D. Lukin, Controlling quantum many-body dynamics in driven rydberg atom arrays, *Science* **371**, 1355 (2021).
- [59] G. Semeghini, H. Levine, A. Keesling, S. Ebadi, T. T. Wang, D. Bluvstein, R. Verresen, H. Pichler, M. Kalinowski, R. Samajdar, A. Omran, S. Sachdev, A. Vishwanath, M. Greiner, V. Vuletić, and M. D. Lukin, Probing topological spin liquids on a programmable quantum simulator, *Science* **374**, 1242 (2021).
- [60] F. Fang, K. Wang, V. S. Liu, Y. Wang, R. Cimmino, J. Wei, M. Bintz, A. Parr, J. Kemp, K.-K. Ni, *et al.*, Probing critical phenomena in open quantum systems using atom arrays, *arXiv:2402.15376* (2024).
- [61] Y. Cheng and H. Zhai, Emergent U(1) lattice gauge theory in Rydberg atom arrays, *Nature Reviews Physics* **6**, 566 (2024).
- [62] X. Wu, Z. Wang, F. Yang, R. Gao, C. Liang, M. K. Tey, X. Li, T. Pohl, and L. You, Dissipative time crystal in a strongly interacting Rydberg gas, *Nature Physics* **20**, 1389 (2024).
- [63] X. Liang, Z. Yue, Y.-X. Chao, Z.-X. Hua, Y. Lin, M. K. Tey, and L. You, Observation of anomalous information scrambling in a Rydberg atom array, *arXiv:2410.16174* (2024).
- [64] N. U. Köylüoglu, N. Maskara, J. Feldmeier, and M. D. Lukin, Floquet engineering of interactions and entanglement in periodically driven rydberg chains, *arXiv:2408.02741* (2024).
- [65] J. S. Waugh, L. M. Huber, and U. Haeberlen, Approach to high-resolution nmr in solids, *Phys. Rev. Lett.* **20**, 180 (1968).
- [66] M. Aidelsburger, M. Atala, M. Lohse, J. T. Barreiro, B. Paredes, and I. Bloch, Realization of the hofstadter hamiltonian with ultracold atoms in optical lattices, *Phys. Rev. Lett.* **111**, 185301 (2013).
- [67] H. Miyake, G. A. Siviloglou, C. J. Kennedy, W. C. Burton, and W. Ketterle, Realizing the harper hamiltonian with laser-assisted tunneling in optical lattices, *Phys. Rev. Lett.* **111**, 185302 (2013).
- [68] N. Goldman and J. Dalibard, Periodically driven quantum systems: Effective hamiltonians and engineered gauge fields, *Phys. Rev. X* **4**, 031027 (2014).
- [69] G. Jotzu, M. Messer, R. Desbuquois, M. Lebrat, T. Uehlinger, D. Greif, and T. Esslinger, Experimental realization of the topological Haldane model with ultracold fermions, *Nature* **515**, 237 (2014).
- [70] L. D. Marin Bukov and A. Polkovnikov, Universal high-frequency behavior of periodically driven systems: from dynamical stabilization to floquet engineering, *Advances in Physics* **64**, 139 (2015).
- [71] F. Meinert, M. J. Mark, K. Lauber, A. J. Daley, and H.-C. Nägerl, Floquet engineering of correlated tunneling in the bose-hubbard model with ultracold atoms, *Phys. Rev. Lett.* **116**, 205301 (2016).
- [72] N. Fläschner, B. S. Rem, M. Tarnowski, D. Vogel, D.-S. Lühmann, K. Sengstock, and C. Weitenberg, Experimental reconstruction of the berry curvature in a floquet bloch band, *Science* **352**, 1091 (2016).
- [73] A. Eckardt, Colloquium: Atomic quantum gases in periodically driven optical lattices, *Rev. Mod. Phys.* **89**, 011004 (2017).
- [74] K. X. Wei, C. Ramanathan, and P. Cappellaro, Exploring localization in nuclear spin chains, *Phys. Rev. Lett.* **120**, 070501 (2018).
- [75] J. Choi, H. Zhou, H. S. Knowles, R. Landig, S. Choi, and M. D. Lukin, Robust dynamic hamiltonian engineering of many-body spin systems, *Phys. Rev. X* **10**, 031002 (2020).
- [76] S. Geier, N. Thaicharoen, C. Hainaut, T. Franz, A. Salzinger, A. Tebben, D. Grimshndl, G. Zürn, and M. Weidemüller, Floquet hamiltonian engineering of an isolated many-body spin system, *Science* **374**, 1149 (2021).
- [77] P. Scholl, H. J. Williams, G. Bornet, F. Wallner, D. Barredo, L. Henriet, A. Signoles, C. Hainaut, T. Franz, S. Geier, A. Tebben, A. Salzinger, G. Zürn, T. Lahaye, M. Weidemüller, and A. Browaeys, Microwave engineering of programmable xxz hamiltonians in arrays of rydberg atoms, *PRX Quantum* **3**, 020303 (2022).
- [78] S. Liu, S.-X. Zhang, C.-Y. Hsieh, S. Zhang, and H. Yao, Discrete time crystal enabled by stark many-body localization, *Phys. Rev. Lett.* **130**, 120403 (2023).
- [79] H. Zhou, L. S. Martin, M. Tyler, O. Makarova, N. Leitao, H. Park, and M. D. Lukin, Robust higher-order hamiltonian engineering for quantum sensing with strongly interacting systems, *Phys. Rev. Lett.* **131**, 220803 (2023).
- [80] S. Geier, A. Braemer, E. Braun, M. Müllenbach, T. Franz, M. Gärttner, G. Zürn, and M. Weidemüller, Time-reversal in a dipolar quantum many-body spin system, *Phys. Rev. Res.* **6**, 033197 (2024).
- [81] W. Buijsman and P. W. Claeys, Weak ergodicity breaking from supersymmetry in a fermionic kinetically constrained model, *arXiv:2412.16287* (2024).
- [82] J. c. v. Minář, B. van Voorden, and K. Schoutens, Kink dynamics and quantum simulation of supersymmetric lattice hamiltonians, *Phys. Rev. Lett.* **128**, 050504 (2022).
- [83] See Supplemental Materials for more details, including

- (I) advantage of demonstrating supersymmetry via supercharge dynamics, (II) comparison with other experimental proposals for SUSY on Rydberg atom arrays, (III) details of initial state preparation and supercharge measurement, (IV) derivation of M_1 model in the spin-1/2 basis, (V) derivation of the effective Floquet Hamiltonian, (VI) details of numerical simulation and additional numerical results.
- [84] N. Maskara, A. A. Michailidis, W. W. Ho, D. Bluvstein, S. Choi, M. D. Lukin, and M. Serbyn, Discrete time-crystalline order enabled by quantum many-body scars: Entanglement steering via periodic driving, *Phys. Rev. Lett.* **127**, 090602 (2021).
- [85] D. V. Else, B. Bauer, and C. Nayak, Prethermal phases of matter protected by time-translation symmetry, *Phys. Rev. X* **7**, 011026 (2017).
- [86] S.-X. Zhang, J. Allcock, Z.-Q. Wan, S. Liu, J. Sun, H. Yu, X.-H. Yang, J. Qiu, Z. Ye, Y.-Q. Chen, C.-K. Lee, Y.-C. Zheng, S.-K. Jian, H. Yao, C.-Y. Hsieh, and S. Zhang, TensorCircuit: a Quantum Software Framework for the NISQ Era, *Quantum* **7**, 912 (2023). <https://github.com/tensorcircuit/tensorcircuit-ng>.
- [87] N. V. Vitanov, A. A. Rangelov, B. W. Shore, and K. Bergmann, Stimulated raman adiabatic passage in physics, chemistry, and beyond, *Rev. Mod. Phys.* **89**, 015006 (2017).
- [88] T. Manovitz, S. H. Li, S. Ebadi, R. Samajdar, A. A. Geim, S. J. Evered, D. Bluvstein, H. Zhou, N. U. Koyluoglu, J. Feldmeier, P. E. Dolgirev, N. Maskara, M. Kalinowski, S. Sachdev, D. A. Huse, M. Greiner, V. Vuletić, and M. D. Lukin, Quantum coarsening and collective dynamics on a programmable simulator, *Nature* **638**, 86 (2025).
- [89] F. Alcaraz and R. Bariev, An exactly solvable constrained xxz chain, Statistical Physics on the Eve of the 21st Century. In Honour of JB McGuire on the Occasion of His 65th Birthday (Series on Advances in Statistical Mechanics), Eds., MT Batchelor, LT Wille (World Scientific, Singapore, 1999). arXiv: cond-mat/9904042 (1999).
- [90] H. Sable, N. M. Myers, and V. W. Scarola, Toward quantum analogue simulation of many-body supersymmetry with rydberg atom arrays, [arXiv:2405.21073](https://arxiv.org/abs/2405.21073) (2024).
- [91] D. W. Schönleber, C. D. B. Bentley, and A. Eisfeld, Engineering thermal reservoirs for ultracold dipole-dipole-interacting rydberg atoms, *New Journal of Physics* **20**, 013011 (2018).
- [92] M. Metcalf, J. E. Moussa, W. A. de Jong, and M. Sarovar, Engineered thermalization and cooling of quantum many-body systems, *Phys. Rev. Res.* **2**, 023214 (2020).

Supplemental Material for “Supersymmetry dynamics on Rydberg atom arrays”

CONTENTS

I. The advantage of demonstrating supersymmetry via supercharge dynamics	9
II. Comparison with other experimental proposals for SUSY on Rydberg atom arrays	10
III. Initial state preparation and supercharge measurement	10
IV. M_1 model with open boundary conditions	11
V. Derivation of the effective Floquet Hamiltonian	12
A. Hamiltonian engineering	12
B. Number operator in the rotated frame	13
C. Effective Floquet Hamiltonian	14
VI. Details of numerical simulation and additional numerical results	17

I. THE ADVANTAGE OF DEMONSTRATING SUPERSYMMETRY VIA SUPERCHARGE DYNAMICS

Besides the constant supercharge expectation value, other quantum dynamics features can also demonstrate supersymmetry. As previously investigated in Ref. [82], if the Hamiltonian H is supersymmetric, the dynamics of the fidelity between the right-most one-kink state and the evolved left-most one-kink state

$$F(t) = |\langle K_r | e^{-iHt} | K_l \rangle|^2, \quad (\text{S1})$$

is identical to the dynamics of the fidelity between the right-most one-skink state and the evolved left-most one-skink state,

$$\tilde{F}(t) = |\langle \tilde{K}_r | e^{-iHt} | \tilde{K}_l \rangle|^2, \quad (\text{S2})$$

where $|\tilde{K}_{l(r)}\rangle$ is the superpartner of $|K_{l(r)}\rangle$. For a normalized eigenstate $|s\rangle$ which satisfies $H|s\rangle = E_s|s\rangle$ and $Q^\dagger|s\rangle = 0$, it is easy to find its superpartner $|\tilde{s}\rangle = Q|s\rangle$. Obviously, $H|\tilde{s}\rangle = E_s|\tilde{s}\rangle$ and $Q|\tilde{s}\rangle = 0$, i.e., $|s\rangle$ and $|\tilde{s}\rangle$ form a doublet. However, $|\tilde{s}\rangle$ is unnormalized because of

$$\langle \tilde{s} | \tilde{s} \rangle = \langle s | Q^\dagger Q | s \rangle = \langle s | H | s \rangle = E_s, \quad (\text{S3})$$

which hinders the preparation of the superpartner of a generic state that is not an energy eigenstate.

We use $|\tilde{s}'\rangle = |\tilde{s}\rangle/\sqrt{E_s}$ to denote the normalized superpartner of $|s\rangle$. In general, the one-kink state or other easily prepared state $|\psi\rangle$ is a superposition of various eigenstates $|s_i\rangle$, i.e., $|\psi\rangle = \sum_i \alpha_i |s_i\rangle$. For simplicity, we assume all eigenstates $|s_i\rangle$ are normalized and satisfy $Q^\dagger|s_i\rangle = 0$. The eigenenergy of $|s_i\rangle$ is $H|s_i\rangle = E_{s_i}|s_i\rangle$. The superpartner of $|\psi\rangle$ is

$$|\tilde{\psi}\rangle = \sum_i \alpha_i |\tilde{s}'_i\rangle = \sum_i \frac{\alpha_i}{\sqrt{E_{s_i}}} |\tilde{s}_i\rangle = \sum_i \frac{\alpha_i}{\sqrt{E_{s_i}}} Q|s_i\rangle = Q \sum_i \frac{\alpha_i}{\sqrt{E_{s_i}}} |s_i\rangle \neq \frac{Q}{z} |\psi\rangle, \quad (\text{S4})$$

where z is the normalization factor $z = \sqrt{\langle \psi | Q^\dagger Q | \psi \rangle} = \sqrt{\sum_i |\alpha_i|^2 E_{s_i}}$. Consequently, we can not straightforwardly apply supercharge operator Q or Q^\dagger to a state to obtain its superpartner. Therefore, the state preparation is challenging for experimentally demonstrating the supersymmetry via the identical fidelity dynamics in different parity sectors. For the one-kink and the corresponding one-skink states considered in Ref. [82], although they can be prepared approximately, an adiabatic evolution with prior knowledge is necessary. In contrast, no high-precision initial state preparation is required for demonstrating supersymmetry dynamics via the expectation value of supercharge and thus our scheme is more friendly for experimental investigation. Please see the subsequent section for a detailed comparison between our work and other experimental proposals for SUSY on Rydberg atom arrays.

II. COMPARISON WITH OTHER EXPERIMENTAL PROPOSALS FOR SUSY ON RYDBERG ATOM ARRAYS

In this section, we provide a detailed comparison between the proposal investigated in this work and other experimental proposals for SUSY on Rydberg atom arrays.

As mentioned above, Ref. [82] proposed exploring the supersymmetry dynamics on Rydberg atom arrays via the identical fidelity dynamics in even and odd parity sectors. Our proposal for investigating supersymmetry dynamics offers several advantages over the one in Ref. [82] for current experimental platforms, particularly in terms of initial state preparation, observable measurement, and experimental setup. 1. Easier initial state preparation. As detailed above, preparing the superpartner of a generic state is inherently challenging. While the specific skink and kink states, which are superpartners, can be prepared in the previous proposal in principle, the task requires an adiabatic evolution. In contrast, our proposal necessitates only pure time-independent Hamiltonian evolution on Rydberg atom arrays for initial state preparation. 2. Easier observable measurement. The former proposal necessitates measuring fidelity to demonstrate supersymmetry dynamics. Our proposal, however, requires only the measurement of Pauli strings, which is much easier than global quantities such as fidelity as further elaborated in the subsequent section. 3. Easier experimental setup. The previous proposal requires the integration of an optical lattice with Rydberg atom manipulation to engineer the supersymmetric Hamiltonian. Our proposal, on the other hand, only requires Floquet engineering, which is a more accessible approach for current experimental setups.

In addition, previous work [28] has demonstrated that the tricritical point of the Ising transition can be achieved on Rydberg atom arrays and proposed to explore the emergent spacetime SUSY on Rydberg atom arrays. Compared to this proposal, our work is also more favorable. 1. No two-qubit digital gate is required in observable measurement in our work while it is inevitable to measure the non-local string operators in the former proposal. 2. Although fine-tuning two parameters is necessary for both proposals, the tuned parameters are analytically trackable in our work. 3. The SUSY characteristics can be revealed solely from dynamics in our case. Although more intriguing spacetime SUSY can be evaluated on ground state, the ground state preparation task is very experimentally challenging, as it requires careful design on adiabatic evolution. Similarly, another work [90] proposed a normalized Witten index as an observable for SUSY and its breaking in supersymmetric lattice models, which can be estimated on Rydberg atom arrays. However, sophisticated engineered thermalization [91, 92] is required which also challenges the experimental demonstration.

III. INITIAL STATE PREPARATION AND SUPERCHARGE MEASUREMENT

In this section, we introduce how to prepare the initial state for supersymmetry dynamics and measure the expectation value of supercharge experimentally.

Starting from a $|g\rangle^{\otimes L}$ state, we can perform Rydberg π pulses on the desired sites to create any product states consistent with blockade constraint, e.g., $\{3j|j \in [1, l]\}$ for $|K_1\rangle$ state considered in the main text. Then we can evolve $|K_1\rangle$ by pure PXP Hamiltonian to generate a superposition state in even and odd parity sectors with non-zero supercharge as the initial state for supersymmetry dynamics. Therefore, the initial state preparation is suitable for the current Rydberg atom array platform.

The supercharge operator shown in Eq. (S6) can be rewritten as

$$\begin{aligned}
Q &= (-1)c_1^\dagger P_2 + \sum_{i=2}^{L-1} (-1)^i P_{i-1} c_i^\dagger P_{i+1} + (-1)^L P_{L-1} c_L^\dagger \\
&= d_1 n_2^d + \sum_{i=2}^{L-1} n_{i-1}^d d_i n_{i+1}^d + n_{L-1}^d d_L \\
&= \frac{\sigma_1^-}{2} \frac{\mathbb{I} + \sigma_2^z}{2} + \sum_{i=2}^{L-1} \frac{\mathbb{I} + \sigma_{i-1}^z}{2} \left(\frac{\sigma_i^-}{2} \prod_{j=1}^{i-1} (-\sigma_j^z) \right) \frac{\mathbb{I} + \sigma_{i+1}^z}{2} + \frac{\mathbb{I} + \sigma_{L-1}^z}{2} \left(\frac{\sigma_L^-}{2} \prod_{j=1}^{L-1} (-\sigma_j^z) \right),
\end{aligned} \tag{S5}$$

where $d_i \equiv (-1)^i c_i^\dagger$ and $n_i^d = d_i^\dagger d_i = P_i$, corresponding to the particle-hole transformation. Therefore, the expectation value of the supercharge can be obtained from the summation of the expectation values of a series of Pauli strings. We can employ the quantum Analog-to-Digital Converter (qADC) [47, 87] that transforms a state in the analogy basis to a digital basis to measure the expectation value of a Pauli string. The analogy basis of Rydberg atom arrays

is $\{|g\rangle, |r\rangle\}$ and the digital basis is $\{|0\rangle, |1\rangle\}$ which can correspond to two hyperfine spin levels of the ground state ($|1\rangle$ is identified as $|g\rangle$). As detailed in Ref. [47], the qADC can be implemented through a coherent mapping protocol. Specifically, we can apply a Raman π pulse to map $|g\rangle$ to $|0\rangle$ and then a subsequent Rydberg π pulse to map $|r\rangle$ to $|1\rangle$. Once the state has been converted to the digital basis, the measurement of any Pauli string is easy via proper single-qubit rotations and computational basis measurements.

IV. M_1 MODEL WITH OPEN BOUNDARY CONDITIONS

In this section, we present the derivation of the Hamiltonian of the M_1 model [33] in the spin-1/2 basis with open boundary conditions. The supercharge operator Q is

$$Q = \sum_{i=1}^L Q_i = (-1)c_1^\dagger P_2 + \sum_{i=2}^{L-1} (-1)^i P_{i-1} c_i^\dagger P_{i+1} + (-1)^L P_{L-1} c_L^\dagger, \quad (\text{S6})$$

where L is the system size, c_i^\dagger (c_i) is the creation (annihilation) operator on i -th site, and $P_i \equiv 1 - c_i^\dagger c_i$ is the projector. Therefore, the Hamiltonian of the M_1 model with open boundary conditions is

$$\begin{aligned} H_{M_1}^{\text{obc}} &= \{Q, Q^\dagger\} \\ &= \left\{ \sum_i Q_i, \sum_j Q_j^\dagger \right\} \\ &= \sum_{i=1}^L \{Q_i, Q_i^\dagger\} + \sum_{i=1}^{L-1} \{Q_i, Q_{i+1}^\dagger\} + \sum_{i=2}^L \{Q_i, Q_{i-1}^\dagger\} \\ &= P_2 + \sum_{i=2}^{L-1} P_{i-1} P_{i+1} + P_{L-1} \\ &\quad - c_1^\dagger c_2 P_3 - \sum_{i=2}^{L-2} P_{i-1} c_i^\dagger c_{i+1} P_{i+2} - P_{L-2} c_{L-1}^\dagger c_L \\ &\quad - c_2^\dagger c_1 P_3 - \sum_{i=2}^{L-2} P_{i-1} c_{i+1}^\dagger c_i P_{i+2} - P_{L-2} c_L^\dagger c_{L-1}. \end{aligned} \quad (\text{S7})$$

We note that the configuration with adjacent fermions is forbidden and the Hilbert space is constrained so that nearest-neighbor sites cannot be simultaneously occupied [34], i.e.,

$$n_i n_{i+1} = 0. \quad (\text{S8})$$

And thus

$$\begin{aligned} H_{M_1}^{\text{obc}} &= n_2^d + \sum_{i=2}^{L-1} n_{i-1}^d n_{i+1}^d + n_{L-1}^d \\ &\quad - (d_1^\dagger d_2 + d_2^\dagger d_1) n_3^d - \sum_{i=2}^{L-2} n_{i-1}^d (d_i^\dagger d_{i+1} + d_{i+1}^\dagger d_i) n_{i+2}^d - n_{L-2}^d (d_{L-1}^\dagger d_L + d_L^\dagger d_{L-1}). \end{aligned} \quad (\text{S9})$$

We can utilize the Jordan-Wigner transformation to map fermionic creation and annihilation operators onto spin operators,

$$\begin{aligned} \sigma_i^z &\equiv 2n_i^d - \mathbb{I}, \\ \frac{1}{2}(\sigma_i^x \sigma_{i+1}^x + \sigma_i^y \sigma_{i+1}^y) &\equiv (d_i^\dagger d_{i+1} + d_{i+1}^\dagger d_i). \end{aligned} \quad (\text{S10})$$

We define the projection operators on the spin basis as

$$\begin{aligned} P_i^r &= \frac{\mathbb{I} + \sigma_i^z}{2}, \\ n_i^r &= \frac{\mathbb{I} - \sigma_i^z}{2}, \end{aligned} \quad (\text{S11})$$

which projects site i onto ground and Rydberg states respectively. Consequently,

$$\begin{aligned}
H_{M_1}^{\text{obc}} &= P_2^r + \sum_{i=2}^{L-1} P_{i-1}^r P_{i+1}^r + P_{L-1}^r \\
&\quad - \frac{1}{2}(\sigma_1^x \sigma_2^x + \sigma_1^y \sigma_2^y) P_3^r - \sum_{i=2}^{L-2} P_{i-1}^r \frac{1}{2}(\sigma_i^x \sigma_{i+1}^x + \sigma_i^y \sigma_{i+1}^y) P_{i+2}^r - P_{L-2}^r \frac{1}{2}(\sigma_{L-1}^x \sigma_L^x + \sigma_{L-1}^y \sigma_L^y) \\
&= \frac{1}{2}(\mathbb{I} + \sigma_2^z) + \sum_{i=2}^{L-1} \frac{1}{4}(\mathbb{I} + \sigma_{i-1}^z + \sigma_{i+1}^z + \sigma_{i-1}^z \sigma_{i+1}^z) + \frac{1}{2}(\mathbb{I} + \sigma_{L-1}^z) - H_{\text{PXY}}^{\text{obc}} \\
&= \frac{1}{4} \sum_{i=2}^{L-1} \sigma_{i-1}^z \sigma_{i+1}^z - H_{\text{PXY}}^{\text{obc}} + \frac{1}{2}(\sigma_2^z + \sigma_{L-1}^z) + \frac{1}{4} \sum_{i=2}^{L-1} (\sigma_{i-1}^z + \sigma_{i+1}^z) + \text{const} \\
&= \frac{1}{4} H_{\text{ZIZ}}^{\text{obc}} - H_{\text{PXY}}^{\text{obc}} - (n_2^r + n_{L-1}^r) - \frac{1}{2} \sum_{i=2}^{L-1} (n_{i-1}^r + n_{i+1}^r) + \text{const} \\
&= \frac{1}{4} H_{\text{ZIZ}}^{\text{obc}} - H_{\text{PXY}}^{\text{obc}} - N + \frac{1}{2}(n_1^r - n_2^r - n_{N-1}^r + n_N^r) + \text{const}.
\end{aligned} \tag{S12}$$

The aforementioned constraint Eq. (S8) corresponds to

$$\begin{aligned}
n_i n_{i+1} &= 0 \\
\Leftrightarrow (1 - n_i^d)(1 - n_{i+1}^d) &= 0 \\
\Leftrightarrow n_i^r n_{i+1}^r &= 0,
\end{aligned} \tag{S13}$$

i.e., the Rydberg blockade.

V. DERIVATION OF THE EFFECTIVE FLOQUET HAMILTONIAN

In this section, we present the detailed derivation of the effective Floquet Hamiltonian H_F with open boundary conditions. For more details, please refer to Ref. [64].

A. Hamiltonian engineering

The Hamiltonian of the driven PXP model with open boundary conditions is

$$H_0^{\text{obc}}(t) = \frac{\Omega}{2} H_{\text{PXP}}^{\text{obc}} - \Delta_0(t) N, \tag{S14}$$

where

$$H_{\text{PXP}}^{\text{obc}} = \sigma_1^x P_2^r + \sum_{i=2}^{L-1} P_{i-1}^r \sigma_i^x P_{i+1}^r + P_{L-1}^r \sigma_L^x, \tag{S15}$$

$$N = \sum_i n_i^r, \tag{S16}$$

and $\Delta_0(t)$ is the time-dependent global detuning given by

$$\Delta_0(t) = \pi \sum_n \delta(t - \frac{\tau}{4} - n \frac{\tau}{2}), \tag{S17}$$

with τ being the Floquet period. It generates a Floquet unitary with period $\tau/2$

$$\begin{aligned}
\chi_{\tau/2} = U_0(\tau/2) &= e^{-i \frac{\tau}{4} \frac{\Omega}{2} H_{\text{PXP}}^{\text{obc}}} e^{i \pi N} e^{-i \frac{\tau}{4} \frac{\Omega}{2} H_{\text{PXP}}^{\text{obc}}} \\
&= e^{i \pi N} e^{+i \frac{\tau}{4} \frac{\Omega}{2} H_{\text{PXP}}^{\text{obc}}} e^{-i \frac{\tau}{4} \frac{\Omega}{2} H_{\text{PXP}}^{\text{obc}}} \\
&= e^{i \pi N},
\end{aligned} \tag{S18}$$

and thus

$$U_0(\tau) = \mathbb{I}, \quad (\text{S19})$$

i.e., the time-dependent detuning (Eq. (S17)) realizes a many-body echo at stroboscopic times $n\tau$. Between stroboscopic times, $0 \leq t < \tau$,

$$U_0(t) = e^{-i\pi N \cdot \mathbb{I}_{\tau/4 \leq t < 3\tau/4}} e^{-it' \frac{\Omega}{2} H_{\text{PXP}}^{\text{obc}}}, \quad (\text{S20})$$

where $t' = t'(t) = ||t - \tau/4| - \tau/2| - \tau/4$ [64].

We consider perturbations around the many-body echo point $H_0(t)$, in the form of additional detuning pulses coupling to the number operator N

$$H(t) = H_0^{\text{obc}}(t) - \tilde{\Delta}(t)N, \quad (\text{S21})$$

where

$$\begin{aligned} \tilde{\Delta}(t) &= (\gamma - \theta) \sum_n \delta(t - n\tau) + \theta \sum_n \delta(t - \frac{\tau}{2} - n\tau) + \epsilon \sum_n \delta(t - \frac{\tau}{4} - n\tau) + \epsilon \sum_n \delta(t - \frac{3\tau}{4} - n\tau) \\ &= \sum_{j,n} \tilde{\Delta}_j \delta(t - t_j - n\tau). \end{aligned} \quad (\text{S22})$$

The associated dynamics can be analyzed in a frame co-rotating with $H_0(t)$,

$$\tilde{H}(t) = -\tilde{\Delta}(t)U_0(t)^\dagger N U_0(t), \quad (\text{S23})$$

and the dynamics coincide with those in the laboratory frame at times $n\tau$ due to Eq. (S19). The number operator in this rotated frame is

$$\begin{aligned} \tilde{N}(t') &= U_0(t)^\dagger N U_0(t) \\ &= e^{it' \frac{\Omega}{2} H_{\text{PXP}}^{\text{obc}}} N e^{-it' \frac{\Omega}{2} H_{\text{PXP}}^{\text{obc}}} \\ &= N + \frac{\Omega}{2} it' [H_{\text{PXP}}^{\text{obc}}, N] - \frac{\Omega^2}{8} (t')^2 [H_{\text{PXP}}^{\text{obc}}, [H_{\text{PXP}}^{\text{obc}}, N]] + \dots, \end{aligned} \quad (\text{S24})$$

and thus

$$\begin{aligned} \tilde{H}(t) &= - \sum_{j,n} \tilde{\Delta}_j \delta(t - t_j - n\tau) \tilde{N}(t'_j) \\ &= - \left((\gamma - \theta) \sum_n \delta(t - n\tau) \tilde{N}(0) + \theta \sum_n \delta(t - \frac{\tau}{2} - n\tau) \tilde{N}(0) + \epsilon \sum_n \delta(t - \frac{\tau}{4} - n\tau) \tilde{N}(\frac{\tau}{4}) + \epsilon \sum_n \delta(t - \frac{3\tau}{4} - n\tau) \tilde{N}(-\frac{\tau}{4}) \right), \end{aligned} \quad (\text{S25})$$

i.e., the pulses at $t_j = (0, \frac{\tau}{2})$ couple to the bare Rydberg number operator $\tilde{N}(0) = N$, while pulses at $t_j = (\frac{\tau}{4}, \frac{3\tau}{4})$ couple to $\tilde{N}(\pm\frac{\tau}{4})$. The stroboscopic dynamics can be described by the Floquet unitary U_F , and

$$U(n\tau) = (U_F)^n, \quad (\text{S26})$$

$$U_F = e^{i\epsilon\tilde{N}(-\frac{\tau}{4})} e^{i\theta\tilde{N}(0)} e^{i\epsilon\tilde{N}(\frac{\tau}{4})} e^{i(\gamma-\theta)\tilde{N}(0)}. \quad (\text{S27})$$

B. Number operator in the rotated frame

As discussed above, the stroboscopic dynamics can be described by the Floquet unitary U_F which can be generated by the global number operator in the rotated frame $\tilde{N}(t')$. We now introduce the derivation of $\tilde{N}(t')$.

In a regime of small Floquet periods $\frac{\Omega\tau}{4} \ll 1$, the number operator shown in Eq. (S24) is

$$\tilde{N}(t') = N + \frac{\Omega}{2} it' [H_{\text{PXP}}^{\text{obc}}, N] - \frac{\Omega^2}{8} (t')^2 [H_{\text{PXP}}^{\text{obc}}, [H_{\text{PXP}}^{\text{obc}}, N]] + \mathcal{O}(\Omega^3\tau^3). \quad (\text{S28})$$

We have

$$\begin{aligned}
[H_{\text{PXP}}^{\text{obc}}, N] &= [H_{\text{PXP}}^{\text{obc}}, \sum_j n_j] \\
&= -\frac{1}{2} \sum_i [H_{\text{PXP}}^{\text{obc}}, \sigma_i^z] \\
&= -\frac{1}{2} \left([\sigma_1^x P_2^r, \sigma_1^z] + \sum_{j=2}^{L-1} [P_{j-1}^r \sigma_j^x P_{j+1}^r, \sigma_j^z] + [P_{L-1}^r \sigma_L^x, \sigma_L^z] \right) \\
&= i H_{\text{PYP}}^{\text{obc}},
\end{aligned} \tag{S29}$$

and

$$\begin{aligned}
[H_{\text{PXP}}^{\text{obc}}, [H_{\text{PXP}}^{\text{obc}}, N]] &= i[H_{\text{PXP}}^{\text{obc}}, H_{\text{PYP}}^{\text{obc}}] \\
&= i[\sigma_1^x, \sigma_1^y] P_2^r + i \sum_{j=2}^{L-1} P_{j-1}^r [\sigma_j^x, \sigma_j^y] P_{j+1}^r + i P_{L-1}^r [\sigma_L^x, \sigma_L^y] \\
&\quad + i[\sigma_1^x P_2^r, P_1^r \sigma_2^y] P_3^r + i \sum_{j=2}^{L-2} P_{j-1}^r [\sigma_j^x P_{j+1}^r, P_j^r \sigma_{j+1}^y] P_{j+2}^r + i P_{L-2}^r [\sigma_{L-1}^x P_L^r, P_{L-1}^r \sigma_L^y] \\
&\quad + i[P_1^r \sigma_2^x, \sigma_1^y P_2^r] P_3^r + i \sum_{j=3}^{L-1} P_{j-2}^r [P_{j-1}^r \sigma_j^x, \sigma_{j-1}^y P_j^r] P_{j+1}^r + i P_{L-2}^r [P_{L-1}^r \sigma_L^x, \sigma_{L-1}^y P_L^r].
\end{aligned} \tag{S30}$$

Because

$$\begin{aligned}
[\sigma_j^x, \sigma_j^y] &= 2i\sigma_j^z, \\
[\sigma_{j-1}^x P_j^r, P_{j-1}^r \sigma_j^y] &= -\frac{i}{2}(\sigma_{j-1}^x \sigma_j^x + \sigma_{j-1}^y \sigma_j^y), \\
[P_{j-1}^r \sigma_j^x, \sigma_{j-1}^y P_j^r] &= -\frac{i}{2}(\sigma_{j-1}^x \sigma_j^x + \sigma_{j-1}^y \sigma_j^y),
\end{aligned} \tag{S31}$$

and thus Eq. (S30) is

$$\begin{aligned}
[H_{\text{PXP}}^{\text{obc}}, [H_{\text{PXP}}^{\text{obc}}, N]] &= -2(\sigma_1^z P_2^r + \sum_{j=2}^{L-1} P_{j-1}^r \sigma_j^z P_{j+1}^r + P_{L-1}^r \sigma_L^z) \\
&\quad + (\sigma_1^x \sigma_2^x + \sigma_1^y \sigma_2^y) P_3^r + \sum_{j=2}^{L-2} P_{j-1}^r (\sigma_j^x \sigma_{j+1}^x + \sigma_j^y \sigma_{j+1}^y) P_{j+2}^r + P_{L-2}^r (\sigma_{L-1}^x \sigma_L^x + \sigma_{L-1}^y \sigma_L^y) \\
&= -2H_{\text{PZP}}^{\text{obc}} + 2H_{\text{PXPY}}^{\text{obc}}.
\end{aligned} \tag{S32}$$

Therefore, the number operator in the rotated frame shown in Eq. (S28) is

$$\tilde{N}(t') \approx N - \frac{\Omega}{2} t' H_{\text{PYP}}^{\text{obc}} + \frac{\Omega^2}{4} (t')^2 (H_{\text{PZP}}^{\text{obc}} - H_{\text{PXPY}}^{\text{obc}}). \tag{S33}$$

C. Effective Floquet Hamiltonian

For small perturbations, the Floquet unitary U_F is well-described by a static effective Floquet Hamiltonian,

$$U_F \approx e^{-iH_F\tau}. \tag{S34}$$

The leading order contributions to the effective Floquet Hamiltonian can be obtained by a Floquet-Magnus expansion with

$$\begin{aligned}
H_F^{(0)} &= \sum_j -\frac{\tilde{\Delta}_j}{\tau} \tilde{N}(t'_j), \\
H_F^{(1)} &= \sum_{j>l} \frac{\tilde{\Delta}_j \tilde{\Delta}_l}{2i\tau} [\tilde{N}(t'_j), \tilde{N}(t'_l)].
\end{aligned} \tag{S35}$$

For the specific parameterization of detuning perturbations as shown in Eq. (S22), the associated effective Floquet Hamiltonian is

$$\begin{aligned}\tau H_F^{(0)} &= -\gamma \tilde{N}(0) - \epsilon(\tilde{N}(\frac{\tau}{4}) + \tilde{N}(-\frac{\tau}{4})), \\ \Rightarrow H_F^{(0)} &= -\frac{\gamma}{\tau}N - \frac{\epsilon}{\tau}(2N + \frac{\Omega^2\tau^2}{32}(H_{\text{PZP}}^{\text{obc}} - H_{\text{PXYP}}^{\text{obc}})), \\ &= -\frac{(\gamma + 2\epsilon)}{\tau}N - \frac{\epsilon\Omega^2\tau}{32}(H_{\text{PZP}}^{\text{obc}} - H_{\text{PXYP}}^{\text{obc}}),\end{aligned}\quad (\text{S36})$$

and

$$2i\tau H_F^{(1)} = \epsilon(\gamma - 2\theta)[\tilde{N}(0), \tilde{N}(-\frac{\tau}{4})] + \epsilon\gamma[\tilde{N}(0), \tilde{N}(\frac{\tau}{4})] + \epsilon^2[\tilde{N}(-\frac{\tau}{4}), \tilde{N}(\frac{\tau}{4})]. \quad (\text{S37})$$

We have

$$\begin{aligned}[\tilde{N}(0), \tilde{N}(-\frac{\tau}{4})] &= [N, N + \frac{\Omega\tau}{8}H_{\text{PYP}}^{\text{obc}} + \frac{\Omega^2\tau^2}{64}(H_{\text{PZP}}^{\text{obc}} - H_{\text{PXYP}}^{\text{obc}})], \\ &= [N, \frac{\Omega\tau}{8}H_{\text{PYP}}^{\text{obc}} - \frac{\Omega^2\tau^2}{64}H_{\text{PXYP}}^{\text{obc}}] \\ &= i\frac{\Omega\tau}{8}H_{\text{PXP}}^{\text{obc}},\end{aligned}\quad (\text{S38})$$

because

$$\begin{aligned}[N, H_{\text{PXYP}}^{\text{obc}}] &= 0 \\ \Leftrightarrow [\sigma_j^z, (\sigma_j^x\sigma_{j+1}^x + \sigma_j^y\sigma_{j+1}^y) + (\sigma_{j-1}^x\sigma_j^x + \sigma_{j-1}^y\sigma_j^y)] &= 0.\end{aligned}\quad (\text{S39})$$

Similarly,

$$\begin{aligned}[\tilde{N}(0), \tilde{N}(\frac{\tau}{4})] &= [N, N - \frac{\Omega\tau}{8}H_{\text{PYP}}^{\text{obc}} + \frac{\Omega^2\tau^2}{64}(H_{\text{PZP}}^{\text{obc}} - H_{\text{PXYP}}^{\text{obc}})], \\ &= [N, -\frac{\Omega\tau}{8}H_{\text{PYP}}^{\text{obc}}] \\ &= -i\frac{\Omega\tau}{8}H_{\text{PXP}}^{\text{obc}},\end{aligned}\quad (\text{S40})$$

$$\begin{aligned}[\tilde{N}(-\frac{\tau}{4}), \tilde{N}(\frac{\tau}{4})] &= [N + \frac{\Omega\tau}{8}H_{\text{PYP}}^{\text{obc}} + \frac{\Omega^2\tau^2}{64}(H_{\text{PZP}}^{\text{obc}} - H_{\text{PXYP}}^{\text{obc}}), N - \frac{\Omega\tau}{8}H_{\text{PYP}}^{\text{obc}} + \frac{\Omega^2\tau^2}{64}(H_{\text{PZP}}^{\text{obc}} - H_{\text{PXYP}}^{\text{obc}})] \\ &\approx [N, -\frac{\Omega\tau}{8}H_{\text{PYP}}^{\text{obc}}] + [\frac{\Omega\tau}{8}H_{\text{PYP}}^{\text{obc}}, N] \\ &= -i\frac{\Omega\tau}{4}H_{\text{PXP}}^{\text{obc}}.\end{aligned}\quad (\text{S41})$$

Consequently,

$$\begin{aligned}H_F^{(1)} &= \frac{1}{2\tau}(\epsilon(\gamma - 2\theta) - \epsilon\gamma - 2\epsilon^2)\frac{\Omega\tau}{8}H_{\text{PXP}}^{\text{obc}} \\ &= (-\epsilon\theta - \epsilon^2)\frac{\Omega}{8}H_{\text{PXP}}^{\text{obc}}.\end{aligned}\quad (\text{S42})$$

The effective Floquet Hamiltonian is

$$\begin{aligned}H_F &= H_F^{(0)} + H_F^{(1)} \\ &= -\frac{(\gamma + 2\epsilon)}{\tau}N - \frac{\epsilon\Omega^2\tau}{32}(H_{\text{PZP}}^{\text{obc}} - H_{\text{PXYP}}^{\text{obc}}) - (\epsilon\theta + \epsilon^2)\frac{\Omega}{8}H_{\text{PXP}}^{\text{obc}}.\end{aligned}\quad (\text{S43})$$

Moreover,

$$\begin{aligned}
H_{\text{PZP}}^{\text{obc}} &= \sigma_1^z P_2^r + \sum_{i=2}^{L-1} P_{i-1}^r \sigma_i^z P_{i+1}^r + P_{L-1}^r \sigma_L^z \quad (\text{S44}) \\
&= \sigma_1^z \frac{\mathbb{I} + \sigma_2^z}{2} + \sum_{i=2}^{L-1} \frac{\mathbb{I} + \sigma_{i-1}^z}{2} (1 - 2n_i^r) \frac{\mathbb{I} + \sigma_{i+1}^z}{2} + \frac{\mathbb{I} + \sigma_{L-1}^z}{2} \sigma_L^z \\
&= \frac{1}{4} H_{\text{ZIZ}}^{\text{obc}} + \frac{\sigma_1^z + \sigma_L^z}{2} + \frac{\sigma_1^z \sigma_2^z + \sigma_{L-1}^z \sigma_L^z}{2} + \frac{1}{4} \sum_{i=2}^{L-1} (1 - 2n_i^r + \sigma_{i-1}^z + \sigma_{i+1}^z - 2\sigma_{i-1}^z n_i^r - 2n_i^r \sigma_{i+1}^z - 2\sigma_{i-1}^z n_i^r \sigma_{i+1}^z) \\
&= \frac{1}{4} H_{\text{ZIZ}}^{\text{obc}} + \frac{(1 - 2n_1^r) + (1 - 2n_L^r)}{2} + \frac{(1 - 2n_1^r)(1 - 2n_2^r) + (1 - 2n_{L-1}^r)(1 - 2n_L^r)}{2} \\
&\quad - \frac{1}{2} \sum_{i=2}^{L-1} n_i^r + \frac{1}{4} \sum_{i=2}^{L-1} (1 - 2n_{i-1}^r + 1 - 2n_{i+1}^r) - \frac{1}{2} \sum_{i=2}^{L-1} ((1 - 2n_{i-1}^r) n_i^r + n_i^r (1 - 2n_{i+1}^r)) \\
&\quad - \frac{1}{2} \sum_{i=2}^{L-1} (1 - 2n_{i-1}^r) n_i^r (1 - 2n_{i+1}^r) + \text{const} \\
&= \frac{1}{4} H_{\text{ZIZ}}^{\text{obc}} - 2n_1^r - n_2^r - n_{L-1}^r - 2n_L^r + 2n_1^r n_2^r + 2n_{L-1}^r n_L^r - \frac{1}{2} \sum_{i=2}^{L-1} (4n_i^r + n_{i-1}^r + n_{i+1}^r) \\
&\quad + \sum_{i=2}^{L-1} 2(n_{i-1}^r n_i^r + n_i^r n_{i+1}^r - n_{i-1}^r n_i^r n_{i+1}^r) + \text{const.}
\end{aligned}$$

As discussed above, $n_i^r n_{i+1}^r$ is zero in the constraint Hilbert space (Eq. (S13)) and thus

$$H_{\text{PZP}}^{\text{obc}} = \frac{1}{4} H_{\text{ZIZ}}^{\text{obc}} - 3N + \frac{1}{2}(n_1^r - n_2^r - n_{L-1}^r + n_L^r), \quad (\text{S45})$$

up to an unimportant constant.

Therefore, the effective Floquet Hamiltonian (see Eq. (S43)) is

$$\begin{aligned}
H_F &= -\frac{(\gamma + 2\epsilon)}{\tau} N - \frac{\epsilon \Omega^2 \tau}{32} ((\frac{1}{4} H_{\text{ZIZ}}^{\text{obc}} - 3N + \frac{1}{2}(n_1^r - n_2^r - n_{L-1}^r + n_L^r)) - H_{\text{PXY}}^{\text{obc}}) - \frac{\epsilon(\epsilon + \theta)\Omega}{8} H_{\text{PXP}}^{\text{obc}} \quad (\text{S46}) \\
&= -\left(\frac{\gamma + 2\epsilon}{\tau} - \frac{3\epsilon \Omega^2 \tau}{32}\right) N - \left(-\frac{\epsilon \Omega^2 \tau}{32}\right) H_{\text{PXY}}^{\text{obc}} + \frac{1}{4} \left(-\frac{\epsilon \Omega^2 \tau}{32}\right) H_{\text{ZIZ}}^{\text{obc}} + \frac{1}{2} \left(-\frac{\epsilon \Omega^2 \tau}{32}\right) (n_1^r - n_2^r - n_{L-1}^r + n_L^r) \\
&\quad - \frac{\epsilon(\epsilon + \theta)\Omega}{8} H_{\text{PXP}}^{\text{obc}}.
\end{aligned}$$

We set

$$\begin{aligned}
J &= \frac{\gamma + 2\epsilon}{\tau} - \frac{3\epsilon \Omega^2 \tau}{32}, \\
h &= -\frac{\epsilon \Omega^2 \tau}{32}, \\
g &= -\frac{\epsilon(\epsilon + \theta)\Omega}{8}.
\end{aligned} \quad (\text{S47})$$

Then

$$H_F = -JN - h H_{\text{PXY}}^{\text{obc}} + \frac{h}{4} H_{\text{ZIZ}}^{\text{obc}} + \frac{h}{2}(n_1^r - n_2^r - n_{L-1}^r + n_L^r)) + g H_{\text{PXP}}^{\text{obc}}. \quad (\text{S48})$$

When $\theta = -\epsilon$ and $\gamma = \epsilon(\frac{\Omega^2 \tau^2}{16} - 2)$, $g = 0$, $J = h = -\frac{\epsilon \Omega^2 \tau}{32}$, and,

$$H_F = -JN - J H_{\text{PXY}}^{\text{obc}} + \frac{J}{4} H_{\text{ZIZ}}^{\text{obc}} + \frac{J}{2}(n_1^r - n_2^r - n_{N-1}^r + n_N^r)), \quad (\text{S49})$$

which is the same as the Hamiltonian of the one-dimensional M_1 model with open boundary conditions shown in Eq. (S12).

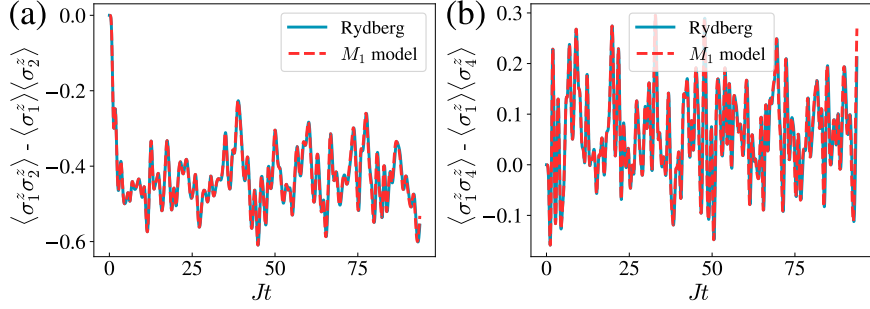


FIG. S1. The dynamics of zz correlation: $\langle \sigma_i^z \sigma_j^z \rangle - \langle \sigma_i^z \rangle \langle \sigma_j^z \rangle$. (a) $i = 1$ and $j = 2$, (b) $i = 1$ and $j = 4$. Here, we set $L = 13$, $\tau = 0.001$, $\frac{\Omega\tau}{4} = 0.025$, $\epsilon = -0.1$. The numerical results evolved by the M_1 model (red) agree well with those of the Rydberg atom array (blue).

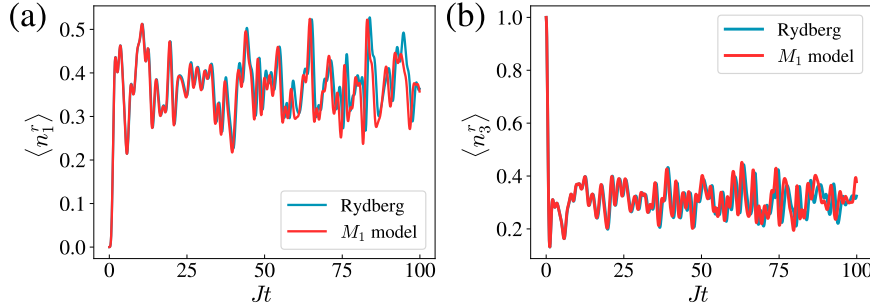


FIG. S2. The Rydberg state density dynamics on site 1 (a) and 3 (b) respectively. Here, we set $L = 13$, $\tau = 0.001$, $\frac{\Omega\tau}{4} = 0.1$, $\epsilon = -0.2$. The numerical results evolved by the M_1 model (red) agree well with those of the Rydberg atom array (blue) in the early times.

VI. DETAILS OF NUMERICAL SIMULATION AND ADDITIONAL NUMERICAL RESULTS

We employ the python package `TensorCircuit` [86] to perform numerical simulations for Hamiltonian dynamics. As discussed above, we set

$$\begin{aligned} \theta &= -\epsilon, \\ \gamma &= \epsilon \left(\frac{\Omega^2 \tau^2}{16} - 2 \right). \end{aligned} \quad (\text{S50})$$

To demonstrate the correspondence between the stroboscopic dynamics of the driven PXP model under Floquet engineering and the supersymmetric M_1 model, we also calculated the zz correlation $\langle \sigma_i^z \sigma_j^z \rangle - \langle \sigma_i^z \rangle \langle \sigma_j^z \rangle$. As shown in Fig S1, the results also coincide. Moreover, we also compared the stroboscopic dynamics of the driven PXP model with larger $\frac{\Omega\tau}{4}$ and the dynamics of the M_1 model, as shown in Fig. S2 and Fig. S3. The deviation appears much earlier than that shown in the main text due to the larger $\frac{\Omega\tau}{4}$, consistent with the theoretical prediction on the approximation error.

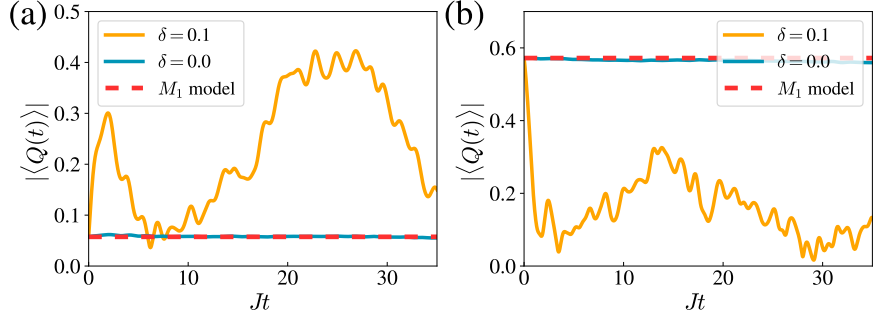


FIG. S3. Supercharge dynamics with (a) $t^* = 5$ and (b) $t^* = 10$. Here, we set $L = 13$, $\tau = 0.001$, $\frac{\Omega\tau}{4} = 0.05$, $\epsilon = -0.1$, and $\theta = -(1 + \delta)\epsilon$. The expectation value of supercharge is the same as that under the quench of M_1 model and is a constant when $\delta = 0.0$. At the same time, the supercharge dynamics is nonconserved when $\delta \neq 0.0$, i.e., the effective Floquet Hamiltonian is nonsupersymmetric. We note that the accumulated approximation errors induce the deviation at late times even with $\delta = 0$.